A new wrapper for a reliable resolution of underdetermined nonlinear equations

Luc Jaulin

July 24, 2026

Abstract

This paper introduces a new wrapper called a *gutter*, designed to enclose sections of the solution set defined by underdetermined nonlinear equations. We demonstrate that, compared to existing wrappers, gutters can provide a more accurate outer approximation with lower computational cost. Several examples from the literature illustrate the efficiency and accuracy of this approach.

1 Introduction

In this paper, we want to characterize the set

$$\mathbb{X} = \{\mathbf{x} \in [\mathbf{x}] | \mathbf{f}(\mathbf{x}) = \mathbf{0}\} \tag{1}$$

where $\mathbf{x} \in \mathbb{R}^n$ and $\mathbf{f}(\mathbf{x}) \in \mathbb{R}^m$ is a nonlinear differentiable function. We assume that we have an undetermined system of equations, *i.e.*, $m < n$. This type of problems has already been considered by several authors using interval based methods [16] [20] [22]. Existing interval-based methods for solving equations [12] [18] rely on different types of wrappers to enclose the solution set. The simplest choice consists of interval boxes [7] [17], which are easy to bisect, project and combine into non-overlapping pavings, but they only provide zeroth-order approximations and therefore require a large number of subdivisions to achieve a high accuracy. More sophisticated wrappers, such as polyhedra, ellipsoids, parallelotopes or zonotopes, can exploit first-order information and significantly improve the local approximation. However, they generally lose one or more properties that are essential for branch-and-prune algorithms: guaranteed and inexpensive projection, simple intersection, efficient bisection, or the construction of non-overlapping coverings. As a consequence, current approaches must balance geometric accuracy against computational simplicity. To my knowledge, no existing wrapper simultaneously provides first-order accuracy together with the algorithmic properties required for efficient interval subdivision methods.

The main contribution of this paper is the introduction of a new wrapper, called a *gutter*, designed specifically for the reliable solution of underdetermined nonlinear systems. A gutter combines the simplicity of box-based representations with a first-order affine approximation of the solution manifold. It preserves the ability to perform efficient projection, intersection and bisection while providing a guaranteed first-order enclosure of the solution set. Based on this representation, we introduce *gutter contractors* and show both theoretically and experimentally that they reduce the amount of subdivision required to achieve a prescribed accuracy. Numerical experiments on three benchmark problems illustrate that gutters can produce tighter enclosures with lower computational cost than classical interval approaches, especially when high accuracy is required.

Let us recall the principle of a first-order approach [6] [8] [16], taking a small box $[\mathbf{x}]$ with center $\bar{\mathbf{x}}$, as illustrated by Figure 1.

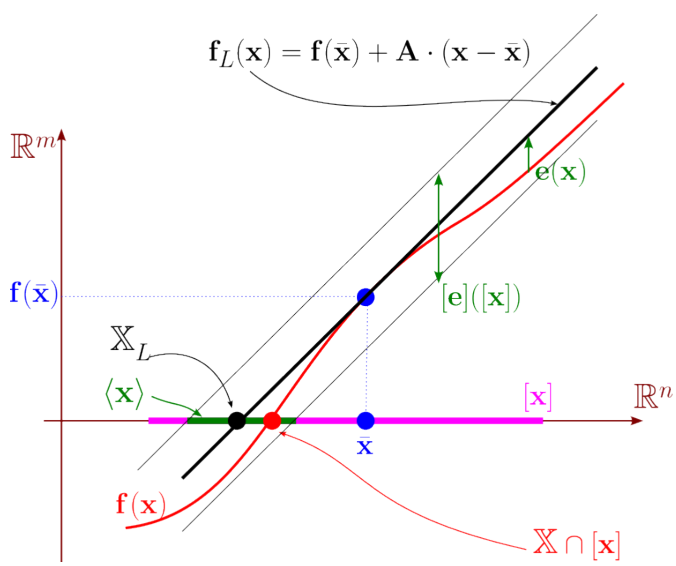

Figure 1: Principle to get a first-order approximation $\langle\mathbf{x}\rangle$ of $\mathbb{X} \cap [\mathbf{x}]$

On this small box, we build the following linear approximation:

$$\mathbf{f}(\mathbf{x}) \simeq \underbrace{\mathbf{f}(\bar{\mathbf{x}}) + \mathbf{A} \cdot (\mathbf{x} - \bar{\mathbf{x}})}_{\mathbf{f}_L(\mathbf{x})} \tag{2}$$

where $\mathbf{A} = \frac{d\mathbf{f}}{d\mathbf{x}}(\bar{\mathbf{x}})$. The linear approximation set for $\mathbb{X}$:

$$\mathbb{X}_L = \{\mathbf{x} \in [\mathbf{x}] | \mathbf{f}_L(\mathbf{x}) = \mathbf{0}\} \tag{3}$$

is valid on the box $[\mathbf{x}]$. Equivalently, we can write

$$\mathbb{X} \cap [\mathbf{x}] \simeq \mathbb{X}_L \cap [\mathbf{x}] \tag{4}$$

Now, this approximation is not reliable. Indeed, even if the error

$$\mathbf{e}(\mathbf{x}) = \mathbf{f}_L(\mathbf{x}) - \mathbf{f}(\mathbf{x}) \tag{5}$$

is small for all $\mathbf{x} \in [\mathbf{x}]$, we cannot conclude that $\mathbb{X} \cap [\mathbf{x}]$ and $\mathbb{X}_L \cap [\mathbf{x}]$ are close. For instance if $\mathbf{f}(\mathbf{x}) = \mathbf{0}$ for all $\mathbf{x} \in [\mathbf{x}]$ and we can always find $\mathbf{f}_L(\mathbf{x})$ (for instance, a constant) which is a good approximation for $\mathbf{f}$ but which never vanishes. However, this situation occurs only when the Jacobian of $\mathbf{f}$ is not full rank and can be considered as non-generic.

In this paper, we propose to use this first-order approach to enclose the solution set $\mathbb{X}$. For this, we need to compute a reliable upper bound for the distance between the two sets $\mathbb{X} \cap [\mathbf{x}]$ and $\mathbb{X}_L \cap [\mathbf{x}]$. More precisely, we need to know how much we have to inflate $\mathbb{X}_L$ in order to get an enclosure $\langle \mathbf{x} \rangle$ for $\mathbb{X} \cap [\mathbf{x}]$.

The notion of first-order approximation is taken from [6] where an approximation of order k is said to be obtained if $\mathrm{Vol}(\langle \mathbf{x} \rangle) = O(\varepsilon^n \cdot \varepsilon^{k(n-m)})$, where $\varepsilon = O(w([\mathbf{x}]))$, $w([\mathbf{x}])$ denoting the width of $[\mathbf{x}]$. This is illustrated by Figure 2, in the case $n = 2$, $m = 1$, $k = 1$. We have indeed $\mathrm{Vol}(\langle \mathbf{x} \rangle) = O(\varepsilon^2 \cdot \varepsilon^{1 \cdot (2-1)}) = O(\varepsilon^3)$, whereas $\mathrm{Vol}([\mathbf{x}]) = O(\varepsilon^2)$. Figure 2 illustrates our motivation. A box enclosure ignores the local orientation of the solution manifold and therefore requires many subdivisions to reach high accuracy. A first-order enclosure follows the local tangent, but representing it by a polyhedron may lead to expensive geometric operations. Gutters preserve this first-order information while remaining as easy to manipulate as interval boxes.

A prototype implementation of the proposed gutter approach has been developed using the codac interval library [21] . The implementation used to generate all the numerical experiments presented in this paper is publicly available, allowing the reported results to be reproduced and providing a basis for further developments of the approach.

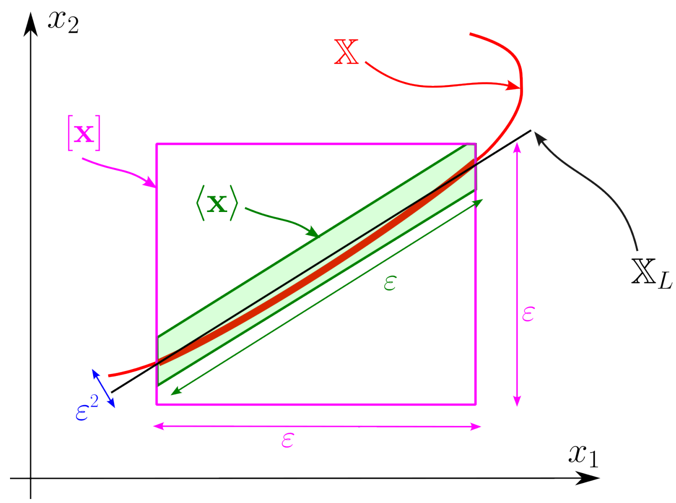

Figure 2: The set $\langle\mathbf{x}\rangle$ is a first-order approximation for $\mathbb{X} \cap [\mathbf{x}]$

This paper is organized as follows. Section 2 recalls the approximation theorem needed to enclose $\mathbb{X} \cap [\mathbf{x}]$ by a polygon for a small box $[\mathbf{x}]$, *i.e.*, for a box with a small width. Section 3 introduces a new type of domain called *gutter*, which is defined by a box $[\mathbf{x}]$, an affine function $\mathbf{Ax} = \mathbf{b}$ (called a *flat*), and a radius ρ. Gutters are easy to handle (project, intersect, ...) still preserving an order one approximation. Section 4 defines the notion of gutter contractors that will be used to approximate accurately the solution set. An illustration of the efficiency of gutters is given in Section 4 on three test cases taken from the literature. Section 6 concludes the paper.

2 Approximation theorem

This section proposes a method to compute an outer approximation of $\mathbb{X} \cap [\mathbf{x}]$ with an order one.

2.1 Parallel linearization

As written previously, to enclose $\mathbb{X} \cap [\mathbf{x}]$, we need first to enclose the graph $\mathbf{f}(\mathbf{x})$ over $[\mathbf{x}]$. This can be done using the parallel linearization (see Section 4.3.4 of [10]). For this, we approximate $\mathbf{f}(\mathbf{x})$ over $[\mathbf{x}]$ by its tangent at the center $\bar{\mathbf{x}}$ of $[\mathbf{x}]$:

$$\mathbf{f}(\mathbf{x}) \simeq \mathbf{f}(\bar{\mathbf{x}}) + \mathbf{A} \cdot (\mathbf{x} - \bar{\mathbf{x}}) \tag{6}$$

The error of this approximation is

$$\mathbf{e}(\mathbf{x}) = \mathbf{f}(\bar{\mathbf{x}}) + \mathbf{A} \cdot (\mathbf{x} - \bar{\mathbf{x}}) - \mathbf{f}(\mathbf{x}) \tag{7}$$

Note that since the approximation corresponds to the tangent of $\mathbf{f}$ at $\bar{\mathbf{x}}$, we have $\mathbf{e}(\bar{\mathbf{x}}) = \mathbf{0}$. An accurate box $[\mathbf{e}]([\mathbf{x}])$ containing $\mathbf{e}(\mathbf{x})$ on $[\mathbf{x}]$ can be obtained using the centered form [16]:

$$[\mathbf{e}]([\mathbf{x}]) = \mathbf{e}(\bar{\mathbf{x}}) + \frac{d\mathbf{e}}{d\mathbf{x}}([\mathbf{x}]) \cdot ([\mathbf{x}] - \bar{\mathbf{x}}) \tag{8}$$

or equivalently , since $\mathbf{e}(\bar{\mathbf{x}}) = \mathbf{0}$,

$$[\mathbf{e}]([\mathbf{x}]) = \left(\mathbf{A} - \frac{d\mathbf{f}}{d\mathbf{x}}([\mathbf{x}])\right) \cdot ([\mathbf{x}] - \bar{\mathbf{x}}) \tag{9}$$

2.2 Polyhedral approximation of $\mathbb{X} \cap [\mathbf{x}]$

Consider the set $\mathbb{X}$, defined by (1) and a box $[\mathbf{x}]$. The following proposition will be used to enclose the set $\mathbb{X} \cap [\mathbf{x}]$ by a polyhedron.

Proposition 1. *We have*

$$\left\{ \begin{array}{c} \mathbf{f}(\mathbf{x}) = \mathbf{0} \\ \mathbf{x} \in [\mathbf{x}] \end{array} \right. \Rightarrow \left\{ \begin{array}{c} \mathbf{A} \cdot \mathbf{x} \in [\mathbf{b}] \\ \mathbf{A} = \frac{d\mathbf{f}}{d\mathbf{x}}(\bar{\mathbf{x}}) \\ [\mathbf{b}] = \mathbf{A}\bar{\mathbf{x}} - \mathbf{f}(\bar{\mathbf{x}}) + [\mathbf{e}] \\ [\mathbf{e}] = \left(\mathbf{A} - \frac{d\mathbf{f}}{d\mathbf{x}}([\mathbf{x}])\right) \cdot ([\mathbf{x}] - \bar{\mathbf{x}}) \end{array} \right. \tag{10}$$

where $\bar{\mathbf{x}}$ *is the center of* $[\mathbf{x}]$.

Proof. For $\mathbf{x} \in [\mathbf{x}]$, from (7) and (9), we have

$$\underbrace{\mathbf{f}(\bar{\mathbf{x}}) + \mathbf{A} \cdot (\mathbf{x} - \bar{\mathbf{x}}) - \mathbf{f}(\mathbf{x})}_{\mathbf{e}(\mathbf{x})} \in \underbrace{\left(\mathbf{A} - \frac{d\mathbf{f}}{d\mathbf{x}}([\mathbf{x}])\right) \cdot ([\mathbf{x}] - \bar{\mathbf{x}})}_{[\mathbf{e}]} \tag{11}$$

Since $\mathbf{f}(\mathbf{x}) = \mathbf{0}$, we get

$$\mathbf{f}(\bar{\mathbf{x}}) + \mathbf{A} \cdot (\mathbf{x} - \bar{\mathbf{x}}) \in [\mathbf{e}] \tag{12}$$

i.e.,

$$\mathbf{A} \cdot \mathbf{x} \in \underbrace{\mathbf{A}\bar{\mathbf{x}} - \mathbf{f}(\bar{\mathbf{x}}) + [\mathbf{e}]}_{[\mathbf{b}]} \tag{13}$$

□

As a consequence, the set $\mathbb{X} \cap [\mathbf{x}]$ is enclosed by the polyhedron defined as the intersection of the box $[\mathbf{x}]$ and the part of the space defined by $\mathbf{A} \cdot \mathbf{x} \in [\mathbf{b}]$. Now, polyhedrons are not easy to handle. For instance computing the projection of a polyhedron or even computing the interval hull is challenging as soon as we want guaranteed results. We prefer instead to use another type of wrapper which is easier to handle and which preserves the first-order approximation, as introduced in the following section.

3 Gutters

A *gutter* is a new type of abstract domain (or *wrapper*) (see [5] for more on abstract domains). Gutters will allow us to compute nonoverlapping paving of a solution set with a first-order approximation. It is not possible to obtain these two features with classical wrappers such as boxes [16], ellipsoids [13], octagons [15], zonotopes [4] [25] or even constrained zonotopes.

As we will see later, the constrained zonotopes used for state estimation [3] [19] [23] are probably the wrappers that most closely resemble *gutters*; however, in their current form, they have not yet been used to solve nonlinear equations.

3.1 Notion of gutter

Definition 1. The *gutter* associated with a box $[\mathbf{x}] \subset \mathbb{R}^n$, a matrix $\mathbf{A}$, a vector $\mathbf{b}$ and the inflation rate ρ is the set $\langle \mathbf{x} \rangle$ defined by

$$\begin{array}{rcl} \langle \mathbf{x} \rangle & = & \langle [\mathbf{x}], \mathbf{A}, \mathbf{b}, \rho \rangle \\ & = & \{\mathbf{x} \in [\mathbf{x}], \exists \mathbf{p}, \mathbf{A}\mathbf{p} = \mathbf{b} \text{ and } \|\mathbf{x} - \mathbf{p}\| < \rho\}\,. \end{array} \tag{14}$$

An illustration is given by Figure 3.

The quantity $\rho = \text{rad}(\langle \mathbf{x} \rangle)$ is called the *radius* of the gutter $\langle \mathbf{x} \rangle$. The affine space $\mathbf{A}\mathbf{p} = \mathbf{b}$ is called a *flat*. The flat defines a sort of *carrier subset* around which $\mathbf{x}$ can exist as soon as there is a point $\mathbf{p}$ of the flat at a distance less than ρ.

Our motivation for using gutters is to have the following properties

- The box $[\mathbf{x}]$ in the structure of the gutter will allow us to build a nonoverlapping covering of $\mathbb{X}$. This is not the case for zonotopes.

- A gutter can easily be bisected, contrary to ellipsoids.
- The axis-aligned projection is easy with gutters, contrary to polyhedrons.
- A first-order approximation is possible, contrary to boxes.

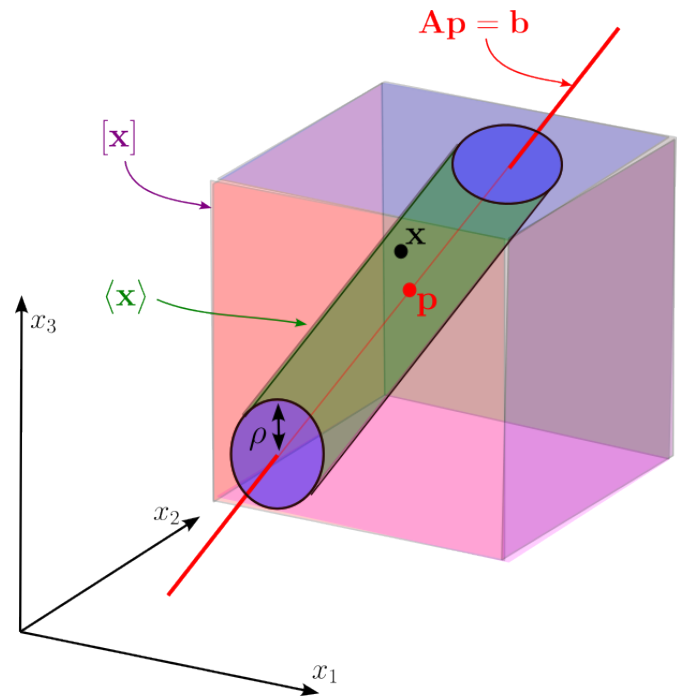

Figure 3: The gutter (green) is here the intersection between the box $[\mathbf{x}]$ and a cylinder

Remark. To understand the benefits of using gutters, consider the initial problem where the set to be characterized $\mathbb{X} = \{\mathbf{x} \in [\mathbf{x}] | \mathbf{f}(\mathbf{x}) = \mathbf{0}\}$ (see Equation 1) is such that function $\mathbf{f}$ is linear, *i.e.*, $\mathbf{f}(\mathbf{x}) = \mathbf{Ax} + \mathbf{b}$. To enclose $\mathbb{X}$ with a high accuracy, we need many boxes (if an approximation with boxes is chosen) whereas a unique gutter $\langle [\mathbf{x}], \mathbf{A}, \mathbf{b}, \rho = 0 \rangle$ is needed. This shows the main advantage of the gutters: even when $\mathbf{f}$ is nonlinear, when the box $[\mathbf{x}]$ is small, the approximation provided by gutters do not suffer from the wrapping effect existing for boxes.

3.2 Axis aligned projection of a gutter

Consider the gutter (see (14)) $\langle \mathbf{x} \rangle = \langle [\mathbf{x}], \mathbf{A}, \mathbf{b}, \rho \rangle$. We rewrite the vector $\mathbf{x}$ as $\mathbf{x} = (\mathbf{x}_1, \mathbf{x}_2) \in \mathbb{R}^n$, with $\mathbf{x}_1 \in \mathbb{R}^m$ and $\mathbf{x}_2 \in \mathbb{R}^{n-m}$.

Definition 2. We define the orthogonal projection of the gutter $\langle\mathbf{x}\rangle = \langle[\mathbf{x}], \mathbf{A}, \mathbf{b}, \rho\rangle$ in the $\mathbf{x}_1$-space as follows

$$\text{proj}_{1:m}(\langle[\mathbf{x}], \mathbf{A}, \mathbf{b}, \rho\rangle) =< [\mathbf{x}_1], \mathbf{A}^{\text{proj}}, \mathbf{b}^{\text{proj}}, \rho > \tag{15}$$

where

$$\begin{array}{ccc} (\mathbf{A}_1, \mathbf{A}_2) & = & \mathbf{A} \\ \mathbf{A}^{\text{proj}} & = & \left(\mathbf{A}_1^{-1}\mathbf{A}_2\right)^{\perp} \\ \mathbf{b}^{\text{proj}} & = & \mathbf{A}^{\text{proj}}\mathbf{A}_1^{-1}\mathbf{b} \\ [\mathbf{x}_1] & = & \text{proj}_{1:m}([\mathbf{x}]) \end{array} \tag{16}$$

In this definition, $\text{proj}_{1:m}$ denotes the orthogonal projection with respect to the first m entries. Figure 4 illustrates the projection in the case where $m = 2$ and $n = 3$.

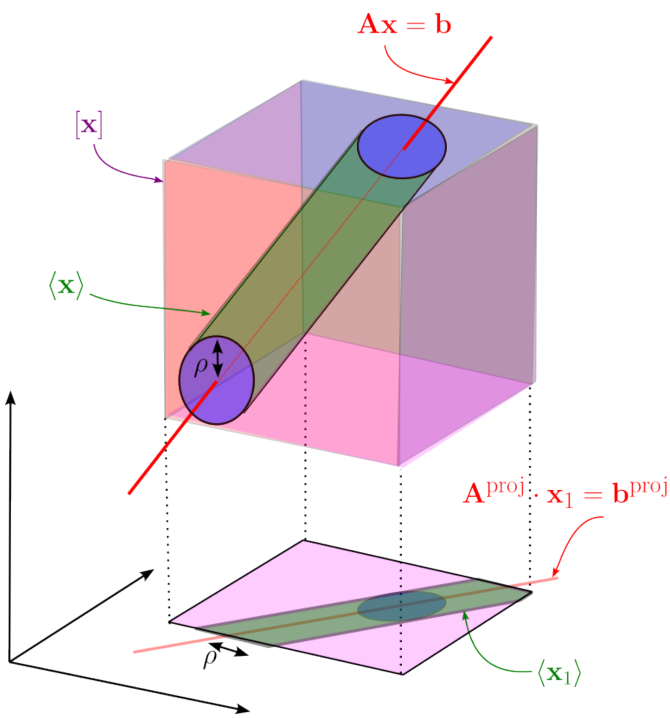

Figure 4: Projection of $\langle\mathbf{x}\rangle$ on the horizontal plane

Proposition 2. *If $\mathbf{x} \in \langle[\mathbf{x}], \mathbf{A}, \mathbf{b}, \rho\rangle$, then $proj_{1:m}\mathbf{x} \in proj_{1:m}(\langle[\mathbf{x}], \mathbf{A}, \mathbf{b}, \rho\rangle)$. See Definition 2 for the projection of a gutter.*

Proof. We have to prove that if $\mathbf{x} \in \langle[\mathbf{x}], \mathbf{A}, \mathbf{b}, \rho\rangle$, then, $\mathbf{x}_1 = \text{proj}_{1:m}\mathbf{x} \in \left\langle[\mathbf{x}_1], \mathbf{A}^{\text{proj}}, \mathbf{b}^{\text{proj}}, \rho\right\rangle$.

(i) The fact that $\mathbf{x}_1 \in [\mathbf{x}_1] \in \text{proj}_{1:m}([\mathbf{x}])$ is trivial.

(ii) Take $\mathbf{x} = (\mathbf{x}_1, \mathbf{x}_2)$ such that $\mathbf{A}\mathbf{x} = \mathbf{b}$. We now check that projection $\mathbf{x}_1$ satisfies

$$\mathbf{A}^{\text{proj}} \cdot \mathbf{x}_1 = \mathbf{b}^{\text{proj}}. \tag{17}$$

We have

$$\mathbf{A}_1\mathbf{x}_1 + \mathbf{A}_2\mathbf{x}_2 = \mathbf{b} \tag{18}$$

i.e.,

$$\mathbf{x}_1 = \mathbf{A}_1^{-1}\mathbf{b} - \mathbf{A}_1^{-1}\mathbf{A}_2\mathbf{x}_2 \tag{19}$$

or equivalently,

$$\underbrace{\mathbf{x}_1 - \mathbf{A}_1^{-1}\mathbf{b}}_{\mathbf{y}} = \underbrace{-\mathbf{A}_1^{-1}\mathbf{A}_2}_{\mathbf{M}} \cdot \underbrace{\mathbf{x}_2}_{\mathbf{b}}. \tag{20}$$

Now, recall that

$$\mathbf{y} = \mathbf{M} \cdot \mathbf{b} \Leftrightarrow \mathbf{N}\mathbf{y} = \mathbf{0} \tag{21}$$

where $\mathbf{N}$ is orthogonal to $\mathbf{M}$, denoted by $\mathbf{N} = \mathbf{M}^{\perp}$. Indeed, if $\mathbf{y}$ is a linear combination of the columns of $\mathbf{M}$ (*i.e.*, $\mathbf{y} = \mathbf{M} \cdot \mathbf{b}$). It means that $\mathbf{y}$ is orthogonal to the null space of $\mathbf{M}$ (*i.e.*, $\mathbf{N}\mathbf{y} = \mathbf{0}$). As a consequence

$$-\left(\mathbf{A}_1^{-1}\mathbf{A}_2\right)^{\perp}\left(\mathbf{x}_1 - \mathbf{A}_1^{-1}\mathbf{b}\right) = \mathbf{0} \tag{22}$$

i.e.,

$$\underbrace{\left(\mathbf{A}_1^{-1}\mathbf{A}_2\right)^{\perp}}_{\mathbf{A}^{\text{proj}}} \cdot \mathbf{x}_1 = \underbrace{\left(\mathbf{A}_1^{-1}\mathbf{A}_2\right)^{\perp} \mathbf{A}_1^{-1}\mathbf{b}}_{\mathbf{b}^{\text{proj}}}. \tag{23}$$

(iii) Take now $\mathbf{x} = (\mathbf{x}_1, \mathbf{x}_2)$ such that $\mathbf{x}$ is at a distance to the flat $\mathbb{P} : \mathbf{A}\mathbf{p} = \mathbf{b}$ less than ρ. Then $\mathbf{x}_1$ is at a distance to $\text{proj}_{1:m}\mathbb{P}$, less that ρ. This is due to the fact that any orthogonal projection is non-expansive, meaning they do not increase distances.

$\square$

Illustration

To explain the procedure, take $m = 2$ and $n = 3$. The system becomes:

$$\underbrace{\begin{pmatrix} a_{11} & a_{12} & a_{13} \\ a_{21} & a_{22} & a_{23} \end{pmatrix}}_{\mathbf{A}} \begin{pmatrix} x_1 \\ x_2 \\ x_3 \end{pmatrix} = \underbrace{\begin{pmatrix} b_1 \\ b_2 \end{pmatrix}}_{\mathbf{b}} \tag{24}$$

After the elimination of x_3 we get

$$(a_{23}a_{11} - a_{13}a_{21})\, x_1 + (a_{23}a_{12} - a_{13}a_{22})\, x_2 \;=\; a_{23}b_1 - a_{13}b_2 \tag{25}$$

Therefore, we can write

$$\mathrm{proj}_{1:2}(\langle [\mathbf{x}], \mathbf{A}, \mathbf{b}, \rho\rangle) = \left\langle [\mathbf{x}_1], \mathbf{A}^{\mathrm{proj}}, b^{\mathrm{proj}}, \rho \right\rangle \tag{26}$$

where

$$\begin{array}{rcl} \mathbf{A}^{\mathrm{proj}} & = & \left(\begin{array}{cc} a_{23}a_{11} - a_{13}a_{21} & a_{23}a_{12} - a_{13}a_{22} \end{array} \right) \\ b^{\mathrm{proj}} & = & a_{23}b_1 - a_{13}b_2 \end{array} \tag{27}$$

3.3 Intersection between two gutters

Following Definition 1, a gutter is a subset of $\mathbb{R}^n$. The intersection of two gutters could follow the classical intersection as defined by set theory. Now, this intersection would yield a set which is not a gutter. To make the intersection closed, we need a definition for the intersection of two gutters $\langle \mathbf{x}_1 \rangle$ and $\langle \mathbf{x}_2 \rangle$ which generates a gutter of $\mathbb{R}^n$ that encloses the set theoretical intersection.

Definition 3. We define the intersection between the two gutters of $\mathbb{R}^n$: $\langle \mathbf{x}_1 \rangle = \langle [\mathbf{x}]_1, \mathbf{A}_1, \mathbf{b}_1, \rho_1 \rangle$ and $\langle \mathbf{x}_2 \rangle = \langle [\mathbf{x}]_2, \mathbf{A}_2, \mathbf{b}_2, \rho_2 \rangle$ as the gutter

$$\langle \mathbf{x}_1 \rangle \cap \langle \mathbf{x}_2 \rangle = \langle [\mathbf{x}]_3, \mathbf{A}_3, \mathbf{b}_3, \rho_3 \rangle \tag{28}$$

with

$$\begin{array}{rcl} [\mathbf{x}]_3 & = & [\mathbf{x}]_1 \cap [\mathbf{x}]_2 \\ \mathbf{A}_3 & = & \left(\begin{array}{c} \mathbf{A}_1 \\ \mathbf{A}_2 \end{array} \right) \\ \mathbf{b}_3 & = & \left(\begin{array}{c} \mathbf{b}_1 \\ \mathbf{b}_2 \end{array} \right) \\ \rho_3 & = & \frac{1}{\sin\theta} \sqrt{\rho_b^2 + \rho_a^2 + 2\rho_a\rho_b \cdot \cos\theta} \end{array} \tag{29}$$

where θ is the principal angle between the two spaces generated by $\mathbf{A}_1$ and $\mathbf{A}_2$.

Figure 5 illustrates the intersection of gutters in the case where $m = 2$ and $n = 3$. To compute θ, we first compute the null space matrices $\mathbf{K}_1, \mathbf{K}_2$ for $\mathbf{A}_1, \mathbf{A}_2$. Then we get

$$\theta = \arcsin \sqrt{1 - \sigma_{\max}^2(\mathbf{K}_1^{\mathrm{T}}\mathbf{K}_2)} \tag{30}$$

where $\sigma_{\max}$ returns the largest singular value.

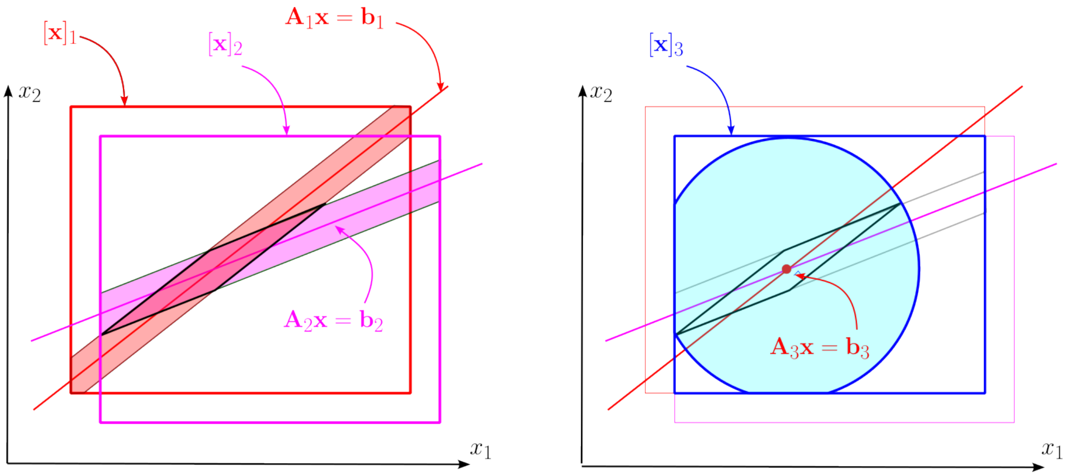

Figure 5: The blue set on the right corresponds to the gutter intersection between the two gutters on the left

Proposition 3. *If* $\mathbf{x} \in \langle \mathbf{x}_1 \rangle$ *and* $\mathbf{x} \in \langle \mathbf{x}_2 \rangle$ *then* $\mathbf{x} \in \langle \mathbf{x}_1 \rangle \cap \langle \mathbf{x}_2 \rangle$.

Proof. The nontrivial point is the radius ρ_3. From the construction of Figure 6, we have

$$\begin{aligned} b \sin\theta &= h_a \\ a \sin\theta &= h_b \end{aligned}$$

Moreover, from the law of cosines, the diameter of the parallelogram is

$$\begin{aligned} d &= \sqrt{a^2 + b^2 + 2ab \cdot |\cos\theta|} \\ &= \sqrt{\frac{h_b^2}{\sin^2\theta} + \frac{h_a^2}{\sin^2\theta} + 2\frac{h_a h_b}{\sin^2\theta} \cdot |\cos\theta|} \\ &= \frac{1}{|\sin\theta|}\sqrt{h_b^2 + h_a^2 + 2h_a h_b \cdot |\cos\theta|} \end{aligned} \tag{31}$$

We conclude that

$$\rho_3 = \frac{1}{\sin\theta}\sqrt{\rho_b^2 + \rho_a^2 + 2\rho_a\rho_b \cdot \cos\theta} \tag{32}$$

$\square$

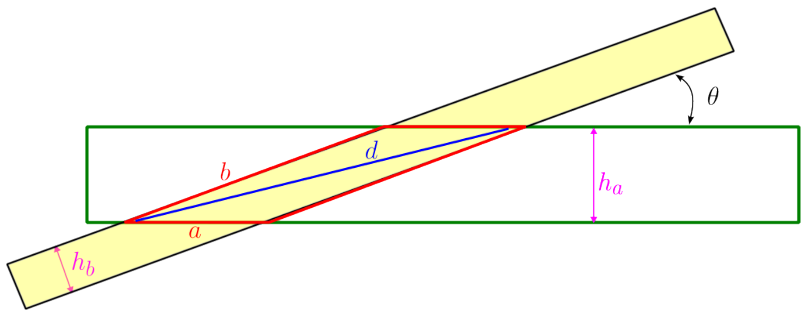

Figure 6: Computation of the diameter of the parallelogram

3.4 Comparison with existing first-order wrappers

Several geometric representations have been proposed to obtain tighter enclosures than interval boxes. Polyhedral enclosures provide accurate first-order approximations of the solution manifold, but geometric operations such as projection, intersection, or the computation of interval hulls generally require dedicated algorithms whose computational cost increases rapidly with the dimension. Parallelotopes and affine enclosures preserve part of the affine structure and can be propagated efficiently, but they are not naturally suited to branch-and-prune algorithms based on non-overlapping pavings. Zonotopes and constrained zonotopes offer compact representations and efficient linear transformations, but exact projection, intersection and subdivision while preserving guaranteed enclosures remain more involved than for interval boxes.

The philosophy of gutters is different. Rather than replacing interval boxes by a richer geometric object, a gutter augments each box with a local affine approximation and a guaranteed inflation radius. As a consequence, the box continues to provide the combinatorial structure required by subdivision algorithms, while the affine component captures the local orientation of the solution manifold. This combination makes it possible to retain first-order approximation properties without sacrificing the simplicity of bisection, axis-aligned projection, or the construction of non-overlapping pavings.

The purpose of gutters is therefore not to compete with general polyhedral or affine representations for arbitrary set computations, but to provide a wrapper specifically designed for the reliable solution of underdetermined nonlinear equations, where repeated subdivision, projection and contraction are the dominant operations.

4 Gutter contractors

Consider again the set

$$\mathbb{X} = \{\mathbf{x} \in \mathbb{R}^n | \mathbf{f}(\mathbf{x}) = \mathbf{0}\} \tag{33}$$

where $\mathbf{f}(\mathbf{x}) \in \mathbb{R}^m$ and $\mathbf{x} \in \mathbb{R}^n$, $m < n$. Take a box $[\mathbf{x}]$. We want to compute a gutter $\langle \mathbf{x} \rangle = \langle [\mathbf{x}], \mathbf{A}, \mathbf{b}, \rho \rangle$ enclosing $\mathbb{X} \cap [\mathbf{x}]$. The radius $\rho = \mathrm{rad}(\langle \mathbf{x} \rangle)$ represents the inflation to be done for the flat $\mathbf{Ax} = \mathbf{b}$ to enclose $\mathbb{X} \cap [\mathbf{x}]$. Equivalently, ρ corresponds to the Hausdorff distance $h(\langle \mathbf{x} \rangle, \mathbb{X} \cap [\mathbf{x}])$ between $\mathbb{X} \cap [\mathbf{x}]$ and $\langle \mathbf{x} \rangle$.

Proposition 4. *Consider the subspace of* $\mathbb{R}^n$

$$\mathbb{E}_0 = \{\mathbf{x} \in \mathbb{R}^n \mid \mathbf{Ax} = \mathbf{0}\}. \tag{34}$$

The orthogonal projection of a vector $\mathbf{y}$ *on* $\mathbb{E}_0$ *is given by*

$$\hat{\mathbf{y}} = \left(\mathbf{I} - \mathbf{A}^T \left(\mathbf{A}\mathbf{A}^T\right)^{-1} \mathbf{A}\right) \mathbf{y}. \tag{35}$$

Proof. Denote by $\mathbf{a}_i$ the vector corresponding to the ith row of $\mathbf{A}$, *i.e.*,

$$\mathbf{A}^{\mathrm{T}} = (\mathbf{a}_1 | \dots | \mathbf{a}_m). \tag{36}$$

The set $\mathbb{E}_0$ corresponds to the set of all $\mathbf{x}$ that are orthogonal to all $\mathbf{a}_j$. Equivalently, the vector space $\mathbb{A} = \mathrm{span}\,(\mathbf{a}_1, \mathbf{a}_2, \dots)$ generated by the $\mathbf{a}_i$, satisfies

$$\mathbb{A} = \mathbb{E}_0^{\perp} \tag{37}$$

and

$$\mathbb{E}_0 = \mathbb{A}^{\perp}. \tag{38}$$

Denote by $\tilde{\mathbf{y}}$ the orthogonal projection of $\mathbf{y}$ on $\mathbb{A}$.

$$\tilde{\mathbf{y}} = \tilde{p}_1 \mathbf{a}_1 + \dots + \tilde{p}_m \mathbf{a}_m = \mathbf{A}^{\mathrm{T}} \tilde{\mathbf{p}} \tag{39}$$

where

$$\tilde{\mathbf{p}} = (\tilde{p}_1, \dots, \tilde{p}_m)^{\mathrm{T}} = \mathrm{argmin} \left\{ \|\mathbf{y} - \mathbf{A}^{\mathrm{T}} \tilde{\mathbf{p}}\|, \mathbf{p} \in \mathbb{R}^m \right\}. \tag{40}$$

Using the least-square formula, we get that

$$\tilde{\mathbf{p}} = \left(\mathbf{A}\mathbf{A}^{\mathrm{T}}\right)^{-1} \mathbf{Ay}, \tag{41}$$

i.e.,

$$\tilde{\mathbf{y}} = \mathbf{A}^{\mathrm{T}} \left(\left(\mathbf{A}\mathbf{A}^{\mathrm{T}} \right)^{-1} \mathbf{A}\mathbf{y} \right) \tag{42}$$

Now, as illustrated by Figure 7, we have $\hat{\mathbf{y}} = \mathbf{y} - \tilde{\mathbf{y}}$. Thus

$$\hat{\mathbf{y}} = \mathbf{y} - \tilde{\mathbf{y}} = \left(\mathbf{I} - \mathbf{A}^{\mathrm{T}} \left(\mathbf{A}\mathbf{A}^{\mathrm{T}} \right)^{-1} \mathbf{A} \right) \mathbf{y}. \tag{43}$$

□

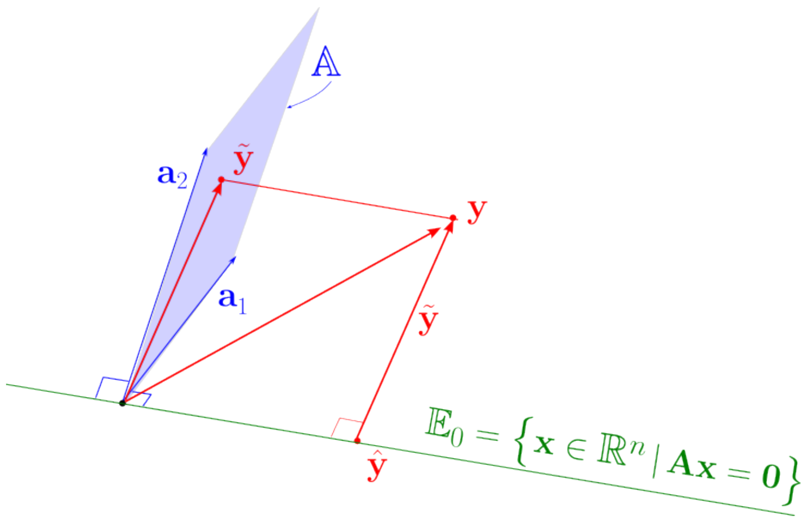

Figure 7: Projection of $\mathbf{y}$ on $\mathbb{E}_0$

Proposition 5. *Consider the two flats of* $\mathbb{R}^n$

$$\begin{array}{rcl} \mathbb{E}_1 & = & \{ \mathbf{x} \in \mathbb{R}^n \,|\, \mathbf{A}\mathbf{x} = \mathbf{b}_1 \} \\ \mathbb{E}_2 & = & \{ \mathbf{x} \in \mathbb{R}^n \,|\, \mathbf{A}\mathbf{x} = \mathbf{b}_2 \} \end{array} \tag{44}$$

The Hausdorff distance [2] between $\mathbb{E}_1$ *and* $\mathbb{E}_2$ *is*

$$h(\mathbb{E}_1, \mathbb{E}_2) = \| \mathbf{A}^T \left(\mathbf{A}\mathbf{A}^T \right)^{-1} (\mathbf{b}_1 - \mathbf{b}_2) \| \tag{45}$$

Figure 8 illustrates the proposition.

Proof. First note that both $\mathbb{E}_1$, $\mathbb{E}_2$ and $\mathbb{E}_0 = \{ \mathbf{x} \in \mathbb{R}^n \,|\, \mathbf{A}\mathbf{x} = \mathbf{0} \}$ are all orthogonal to $\mathbb{A}$. Take one point $\mathbf{x}_1 \in \mathbb{E}_1$. The nearest $\mathbf{x}_2 \in \mathbb{E}_2$ to $\mathbf{x}_1$ is such that the orthogonal projection of $\mathbf{x}_1$ and $\mathbf{x}_2$ on $\mathbb{E}_0$ corresponds to the same point $\mathbf{x}_0$. Equivalently

$$\mathbf{x}_0 = \left(\mathbf{I} - \mathbf{A}^{\mathrm{T}} \left(\mathbf{A}\mathbf{A}^{\mathrm{T}} \right)^{-1} \mathbf{A} \right) \mathbf{x}_1 = \left(\mathbf{I} - \mathbf{A}^{\mathrm{T}} \left(\mathbf{A}\mathbf{A}^{\mathrm{T}} \right)^{-1} \mathbf{A} \right) \mathbf{x}_2. \tag{46}$$

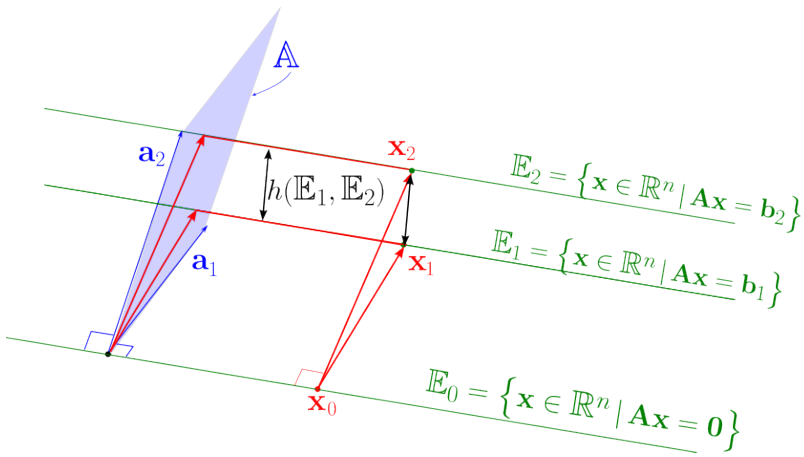

Figure 8: Hausdorff distance between $\mathbb{E}_1$ and $\mathbb{E}_2$

Therefore

$$\mathbf{x}_1 - \mathbf{x}_2 = \mathbf{A}^{\mathrm{T}} \left(\mathbf{A}\mathbf{A}^{\mathrm{T}}\right)^{-1} \mathbf{A} \left(\mathbf{x}_1 - \mathbf{x}_2\right) \tag{47}$$

i.e.,

$$\mathbf{x}_1 - \mathbf{x}_2 = \mathbf{A}^{\mathrm{T}} \left(\mathbf{A}\mathbf{A}^{\mathrm{T}}\right)^{-1} \left(\mathbf{b}_1 - \mathbf{b}_2\right). \tag{48}$$

□

The following proposition tells us how to build a gutter enclosing $\mathbb{X} \cap [\mathbf{x}]$.

Definition 4. Consider a set $\mathbb{X}$ of $\mathbb{R}^n$. A *gutter contractor* $\mathcal{G}$ associated with $\mathbb{X}$ is an operator which takes a box $[\mathbf{x}]$ as input and returns a gutter $\mathcal{G}([\mathbf{x}]) = \langle [\mathbf{x}], \mathbf{A}, \mathbf{b}, \rho \rangle$ such that

$$\mathbb{X} \cap [\mathbf{x}] \;\subset\; \langle [\mathbf{x}], \mathbf{A}, \mathbf{b}, \rho \rangle\,. \tag{49}$$

Moreover, $\mathcal{G}$ is said to have an order k if for all nested sequence of boxes converging to a point $\mathbf{x}$ in $\mathbb{X}$,

$$\frac{h(\mathcal{G}([\mathbf{x}]), \mathbb{X} \cap [\mathbf{x}])}{\mathrm{rad}([\mathbf{x}])^k} \to 0. \tag{50}$$

where $\mathrm{rad}([\mathbf{x}])$ is the radius of the box $[\mathbf{x}]$.

Proposition 6. *Consider the set* $\mathbb{X} = \{\mathbf{x} \in \mathbb{R}^n | \mathbf{f}(\mathbf{x}) = \mathbf{0}\}$. *The operator*

$$\mathcal{G} : [\mathbf{x}] \;\to\; \langle [\mathbf{x}], \mathbf{A}, \mathbf{b}, \rho \rangle \tag{51}$$

where

$$\begin{array}{rcl} \mathbf{b} & = & \mathbf{A}\bar{\mathbf{x}} - \mathbf{f}(\bar{\mathbf{x}}) \\ \mathbf{A} & = & \frac{\partial \mathbf{f}}{\partial \mathbf{x}}(\bar{\mathbf{x}}) \\ \rho & = & \sigma_{\mathbf{A}} \cdot ub(\| \left(\mathbf{A} - \frac{d\mathbf{f}}{d\mathbf{x}}([\mathbf{x}])\right) \cdot ([\mathbf{x}] - \bar{\mathbf{x}})\|) \end{array} \tag{52}$$

is a gutter contractor of order 1. In (52), ub is the upper bound of the corresponding interval and $\sigma_{\mathbf{A}} = \|\mathbf{A}^T \left(\mathbf{A}\mathbf{A}^T\right)^{-1}\|_2$ *is the spectral norm of the matrix* $\mathbf{A}^T \left(\mathbf{A}\mathbf{A}^T\right)^{-1}$*.*

Proof. From Proposition 1, we know that

$$\left\{ \begin{array}{c} \mathbf{f}(\mathbf{x}) = \mathbf{0} \\ \mathbf{x} \in [\mathbf{x}] \end{array} \right. \Rightarrow \left\{ \begin{array}{c} \mathbf{A} \cdot \mathbf{x} = \tilde{\mathbf{b}} \\ \tilde{\mathbf{b}} = \mathbf{A}\bar{\mathbf{x}} - \mathbf{f}(\bar{\mathbf{x}}) + \mathbf{e} \\ \mathbf{e} \in [\mathbf{e}] \end{array} \right. \tag{53}$$

Take $\mathbb{E} : \mathbf{A} \cdot \mathbf{x} = \mathbf{b}$ and $\tilde{\mathbb{E}} : \mathbf{A} \cdot \mathbf{x} = \tilde{\mathbf{b}}$. From Proposition 5,

$$h(\mathbb{E}, \tilde{\mathbb{E}}) = \|\mathbf{A}^{\mathrm{T}} \left(\mathbf{A}\mathbf{A}^{\mathrm{T}}\right)^{-1} \left(\mathbf{b} - \tilde{\mathbf{b}}\right) \| \leq \sigma_{\mathbf{A}} \cdot \|\mathbf{b} - \tilde{\mathbf{b}}\| \tag{54}$$

It means that

$$\begin{array}{l} \exists \mathbf{p} \in \mathbb{R}^n, \mathbf{A} \cdot \mathbf{p} = \mathbf{b} \\ \|\mathbf{p} - \mathbf{x}\| \leq \sigma_{\mathbf{A}} \cdot \|\mathbf{e}\| \end{array} \tag{55}$$

The order 1 for the gutter contractor comes from the fact that

$$\frac{\operatorname{rad}\left(\left(\mathbf{A} - \frac{d\mathbf{f}}{d\mathbf{x}}([\mathbf{x}])\right) \cdot ([\mathbf{x}] - \bar{\mathbf{x}})\right)}{\operatorname{rad}([\mathbf{x}])} \to 0 \tag{56}$$

which is a property of the centered form [16]. □

Remark. In Proposition 6, we assume that the Jacobian ($\mathbf{A} = \frac{\partial \mathbf{f}}{\partial \mathbf{x}}(\bar{\mathbf{x}})$) has full row rank. Under this regularity assumption, the matrix ($\mathbf{A}\mathbf{A}^T$) is positive definite and therefore invertible. The coefficient $\sigma_{\mathbf{A}}$ is thus well defined. When the regularity condition fails (often near singularities), the gutter contractor does not contract anything, reflecting the deterioration of the local conditioning.

5 Test cases

We consider here three test cases from the literature. For each of these test cases, we have to solve a system of 3 variables with two nonlinear equations

$$\begin{array}{rcl} f_1(x_1, x_2, x_3) & = & 0 \\ f_2(x_1, x_2, x_3) & = & 0 \end{array} \tag{57}$$

We want to characterize the set

$$\mathbb{X} = \{(x_1, x_2, x_3) \,|\, \mathbf{f}(x_1, x_2, x_3) = \mathbf{0}\}\,. \tag{58}$$

In the following, the solutions will be depicted on the (x_1, x_2)- space.

5.1 Algorithm

For the resolution, we use a branch and prune algorithm such as SIVIA (see *e.g.* [11]). Now, we take advantage of the gutter contractor $\mathcal{G}$ for the solution set $\mathbb{X} \in \mathbb{R}^3$. A paving with boxes is generated and the current paving is stored in a list $\mathcal{L}$. The final gutters are stored in $\mathbb{X}^+$. The algorithm can be described as follows.

Initialization: $\mathcal{L} = \{[\mathbf{x}]\}$; $\mathbb{X}^+ = \{\}$.

Resolution.

- **Contraction step**. Replace each $[\mathbf{x}] \in \mathcal{L}$, by the smallest box enclosing the gutter $\langle \mathbf{x} \rangle = \mathcal{G}([\mathbf{x}])$.
- **Bisection step**. For each $[\mathbf{x}] \in \mathcal{L}$, if $[\mathbf{x}]$ is too small then push $\langle \mathbf{x} \rangle$ on $\mathbb{X}^+$, otherwise, bisect $[\mathbf{x}]$ and push the two resulting boxes in $\mathcal{L}$.

By too small, we mean

$$\mathrm{rad}([\mathbf{x}]) < \varepsilon \text{ or } \mathrm{rad}(\langle \mathbf{x} \rangle) < 0.01\varepsilon \tag{59}$$

where ε is a small positive number corresponding the desired accuracy. The condition $\mathrm{rad}([\mathbf{x}]) < \varepsilon$ is classical in many interval based algorithm. The condition $\mathrm{rad}(\langle \mathbf{x} \rangle) < 0.01\varepsilon$ tells us that if we have a large box $[\mathbf{x}]$ such that its gutter approximation is already accurate enough, there is no need to bisect it. This condition may drastically reduce the number of generated boxes especially when ε is small.

Moreover, in the definition of the solution set $\mathbb{P}$ (see (58)), we only want to enclose the projection of $\mathbb{X} \subset \mathbb{R}^3$. Each gutter of $\langle \mathbf{x} \rangle$ of $\mathbb{X}^+$ should thus be projected on the (x_1, x_2) space, as explained in Subsection3.2.

5.2 Experimental setup

The objective of the following experimental study is to evaluate the ability of gutter contractors to compute reliable and accurate enclosures of solution manifolds defined by underdetermined nonlinear systems. The three benchmark problems considered in this section were selected because they originate from different application domains (control, robotics and mechanism analysis) and have been used in the interval literature, allowing direct comparison with existing approaches.

All experiments were carried out using a prototype implementation written in Python and based on the codac interval library. Unless otherwise stated, the stopping criterion is controlled by the prescribed accuracy parameter ε, and the branch-and-prune algorithm terminates when either (rad($[\mathbf{x}]$)$<\varepsilon$) or (rad($\langle\mathbf{x}\rangle$) $< 0.01\varepsilon$), as described below. The values of ε used in each experiment are reported together with the corresponding results.

The purpose of these experiments is not to optimize the implementation or demonstrate real-time performance, but rather to assess the geometric quality of the proposed wrapper. Therefore, the main evaluation criteria are (i) the volume of the computed enclosure, which measures the approximation accuracy, and (ii) the computation time required to reach the prescribed accuracy. All computations completed without reaching a timeout.

5.3 Delay system

Consider the linear time-delay system [24] given by

$$\ddot{y} + 2\dot{y}(t - x_1) + y(t - x_2) = 0 \tag{60}$$

where x_1, x_2 are two parameters. Its characteristic function is

$$\theta(x_1, x_2, s) = s^2 + 2se^{-sx_1} + e^{-sx_2}. \tag{61}$$

The location of the roots for $\theta(x_1, x_2, jx_3)$, where $j^2 = -1$ and $s = jx_3$, provides a good understanding of the stability of the system. As in [24], we define the set

$$\{(x_1, x_2) \mid \exists x_3 \in [0, 10],\, \theta(x_1, x_2, jx_3) = 0\}. \tag{62}$$

Since

$$\begin{aligned} & \theta(x_1, x_2, jx_3) = 0 \\ \Leftrightarrow \quad & \mathbf{f}(\mathbf{x}) = \begin{pmatrix} -x_3^2 + 2x_3 \sin(x_3 x_1) + \cos(x_3 x_2) \\ 2x_3 \cos(x_3 x_1) - \sin(x_3 x_2) \end{pmatrix} = \mathbf{0} \end{aligned} \tag{63}$$

the resolution can be done using our algorithm. Different cases have been treated, as illustrated by Table 1. In Figure 9 the lines correspond to different cases (a,b,c,d). The left column shows the paving obtained using one of the best (to my knowledge) interval method with a contractor which is asymptotically minimal [9]. The right column shows the paving obtained by gutter contractors only. Note that for efficiency, the gutter version and the classical interval contractors should be combined. Now, in our examples, the combination does not yield any significant improvements. Several initial boxes have been taken with different accuracy ε. The computing time is denoted by T_1 for the interval contractor and T_2 for the gutter contractor. The volume of the approximation is denoted by V_1 for the interval contractor and V_2 for the gutter contractor. We observe that the improvement becomes significant when ε is small. Indeed, the approximation is more accurate and the computing time is lower. It is a consequence of the first-order approximation of the gutter contractor.

	Case (a)	Case (b)	Case (c)	Case (d)
$[\mathbf{x}]$	$\begin{pmatrix} [0,2] \\ [2,4] \\ [0,10] \end{pmatrix}$	$\begin{pmatrix} [1.3,1.8] \\ [3,3.5] \\ [0,10] \end{pmatrix}$	$\begin{pmatrix} [1.595,1.615] \\ [3.2,3.22] \\ [0,10] \end{pmatrix}$	$\begin{pmatrix} [1.601,1.603] \\ [3.202,3.206] \\ [0,10] \end{pmatrix}$
ε	2^{-4}	2^{-8}	2^{-12}	2^{-16}
$T_1(s)$	0.51	0.84	0.11	0.19
$T_2(s)$	0.86	1.46	0.17	0.05
V_1	0.092	$2.05 \cdot 10^{-3}$	$3.06 \cdot 10^{-6}$	$4.18 \cdot 10^{-7}$
V_2	0.02	$1.93 \cdot 10^{-3}$	$7.2 \cdot 10^{-7}$	$5.78 \cdot 10^{-9}$
$\frac{V_1}{V_2}$	3.8	4.6	15.3	72.4

Table 1. Comparison, for different different levels of accuracy ε between (1) an efficient and accurate interval contractor and (2) the gutter contractor We observe that the improvement due to the gutter contractor becomes significant only when the accuracy becomes high.

Figure 9 provides a graphic comparison between a pure interval approach (left) and a gutter approach (right). The color code is the following. On the left of Figure 9, the blue colored boxes correspond to the approximation of the solution set with boxes and the red frames show the different zooms. On the right of Figure 9, the blue boxes with uncolored insides correspond to the box approximation of the gutters (magenta). Red colored boxes are boxes for which the gutter contractor did not contract anything and that are too small to be bisected.

For Case (a), we observe that the gutters do not yield any improvement. When ε decreases, the approximation becomes increasingly accurate with respect to an interval approximation (represented by the ratio V_1/V_2) and the computational time decreases. In subfigure (a), right, we observe many red boxes. For these boxes, we were unable to get any gutter contraction and only the interval contractor has been efficient. In Subfigure (c), right, the blue boxes on the right are large compared to the left boxes. This is due to the fact that the for the right boxes, the gutter approximation is good enough to be stored in $\mathbb{X}^+$ without any further bisection. In Subfigure (d) right, all blue boxes are such that $\text{rad}(\mathcal{G}([\mathbf{x}])) < 0.01\varepsilon$. The stop criterion $\text{rad}([\mathbf{x}]) < \varepsilon$ is no longer needed. Compared to the classical approach (see Subfigure (d) left), many boxes have to be generated to reach the condition $\text{rad}([\mathbf{x}]) < \varepsilon$. This explains why gutters become much more efficient as soon as a high accuracy is required.

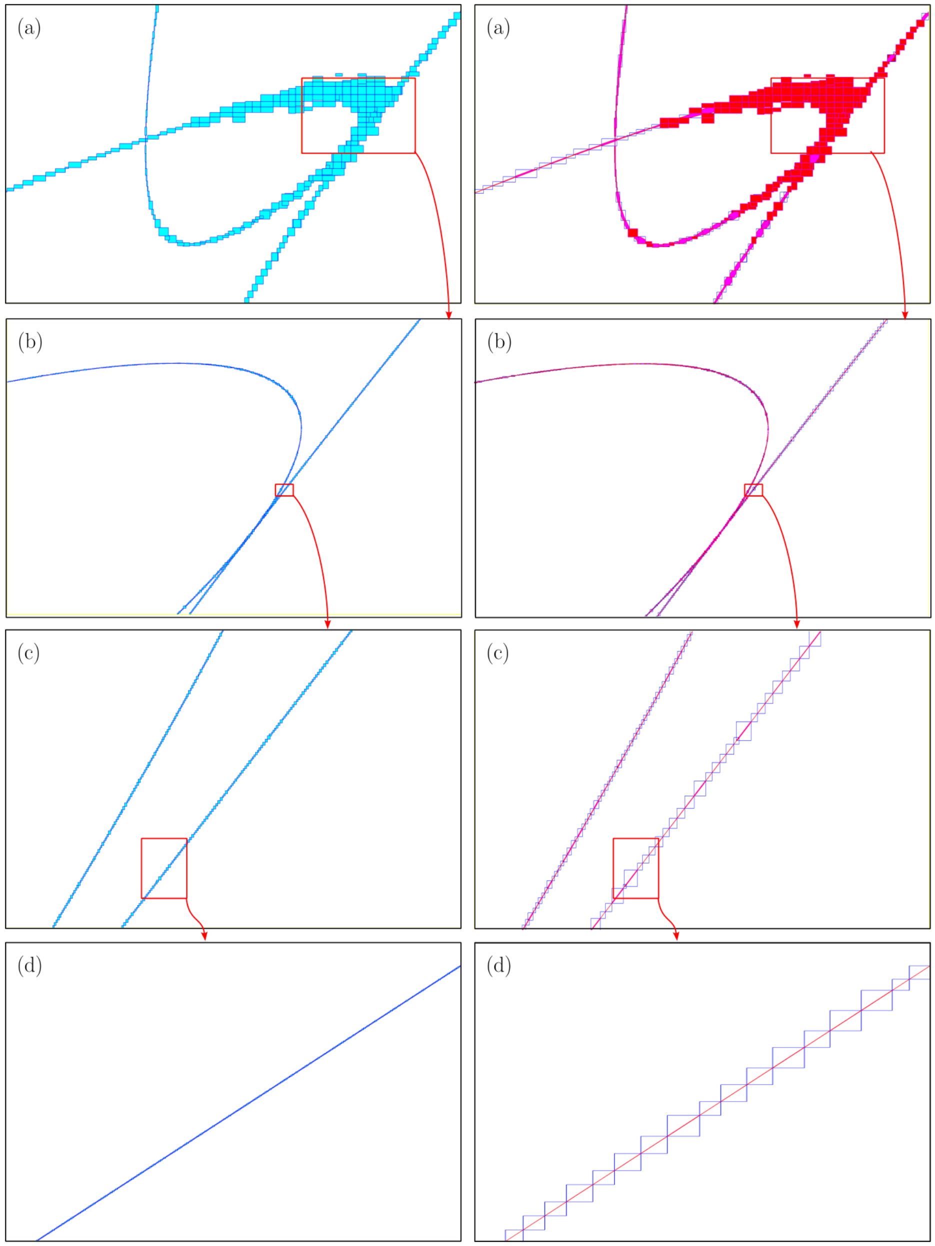

Figure 9: Left: resolution with asymptotically minimal contractors; Right: resolution with gutter contractors. The gutters yields less bisections than classical interval contractors to get a similar accuracy

5.4 Tensegrity

Consider robot described by Figure 10 with three springs (green) and three rigid bars (see [1], pps. 182–183 for more details). The length x_1 of the red rigid bar can be tuned. The magenta bar can slide with no friction along the blue bar.

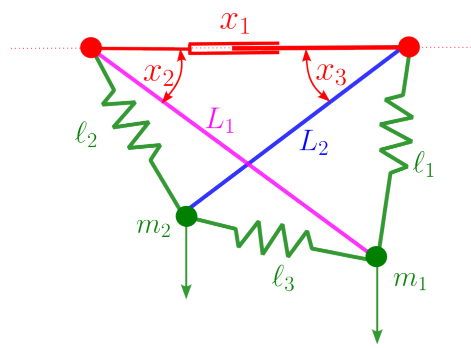

Figure 10: Tensegrity system, only x_1 can be controlled

At the equilibrium, the potential energy U of the mechanism, given by:

$$U = \frac{k}{2}\left(\ell_1^2 + \ell_2^2 + \ell_3^2\right) - m_1 L_1 \sin x_2 - m_2 L_2 \sin x_3 \tag{64}$$

where

$$\begin{aligned} \ell_1^2 &= x_1^2 + L_1^2 - 2x_1 L_1 \cos x_2 \\ \ell_2^2 &= x_1^2 + L_2^2 - 2x_1 L_2 \cos x_3 \\ \ell_3^2 &= (x_1 - L_2 \cos x_3 - L_1 \cos x_2)^2 + (L_2 \sin x_3 - L_1 \sin x_2)^2 \end{aligned} \tag{65}$$

Now, U should be stationary [26], *i.e.*,

$$\begin{aligned} \frac{\partial U}{\partial x_2} &= 0 \\ \frac{\partial U}{\partial x_3} &= 0 \end{aligned} \tag{66}$$

We get

$$\begin{aligned} kL_1 \sin(x_2 + x_3) - 2kx_1 \sin x_3 + m_2 \cos x_3 &= 0 \\ kL_2 \sin(x_2 + x_3) - 2kx_1 \sin x_2 + m_1 \cos x_2 &= 0 \end{aligned} \tag{67}$$

As in [26], we want to characterize the set of all $(x_1, x_2) \in [0,2] \times [-\pi, \pi]$ such that there exists $x_3 \in [-\pi, \pi]$ for which the two equations are satisfied. For $\varepsilon = 2^{-8}$, $L_1 = 1$, $k = 100$, $m_1 = m_2 = 5$, and $L_2 \in \{0.99, 1, 1.05\}$, our algorithm generates Figure 11 (bottom), to be compared with the

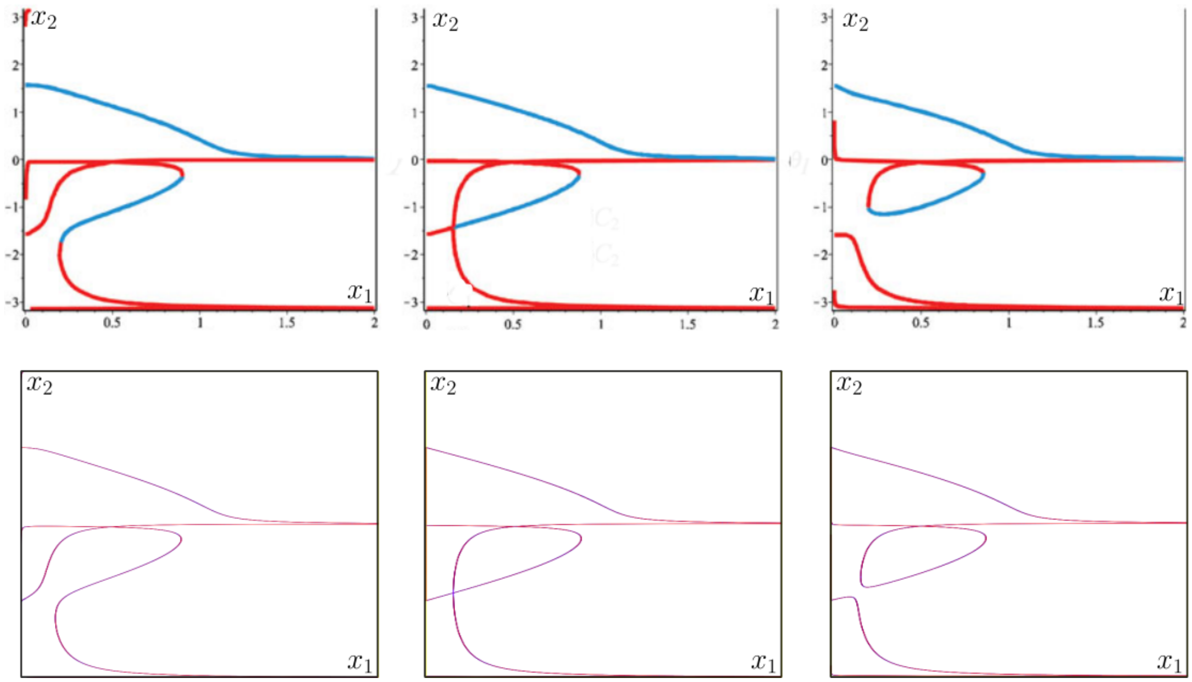

Figure 11: Set of all (x_1, x_2) corresponding to an equilibrium; Top: symbolic approach by Wenger and Chablat; Bottom: with gutters. Left: $L_2 = 0.99$, Center: $L_2 = 1$; Right: $L_2 = 1.05$

symbolic approach of [26]. For our algorithm, the computing time is less than 1sec. No computing time is given in [26].

In the workspace, a discrete approximation of the occupancy set is depicted on Figure 12. This occupancy set has been obtained by discretizing the configuration space approximation produced by the gutter algorithm. For each terminal gutter, a regular grid of configurations is sampled, the corresponding forward kinematics is evaluated, and the resulting workspace points are accumulated.

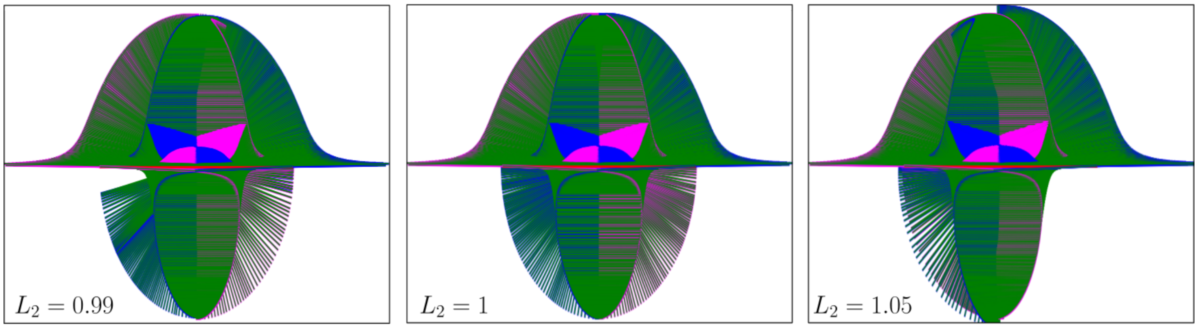

Figure 12: In the workspace, representation of all configurations for the robot, for different values of L_2

5.5 RP-5AH robot

We consider the example taken from [14] with the robot RP-5AH made by Mitsubishi, as illustrated by Figure 13. The parameters are taken as $a_1 = -1$, $a_2 = 0$, $b_1 = 1$, $b_2 = 0$, $\ell_1 = \ell_2 = \frac{3}{2}$, $\ell_3 = \ell_4 = 2$. For this robot, we can control the two angles x_1 and x_2 that are linked by the constraint that the point $\mathbf{p}$ should belong to the Lissajou curve of equation

$$\mathbf{p}(x_3) = \begin{pmatrix} \sin x_3 \\ \frac{3}{2} + \cos(3x_3) \end{pmatrix} \tag{68}$$

for some $x_3 \in [0, 2\pi]$. Equivalently to [14], we want to characterize the set of all (x_1, x_2) such that there exists $x_3 \in [0, 2\pi]$ such that

$$\begin{array}{rcl} (\sin x_3 - \ell_3 \cos x_1 - a_1)^2 + (\frac{3}{2} + \cos(3x_3) - \ell_3 \sin x_1 + a_2)^2 - \ell_1^2 & = & 0 \\ (\sin x_3 - \ell_4 \cos x_2 - b_1)^2 + (\frac{3}{2} + \cos(3x_3) - \ell_4 \sin x_2 - b_2)^2 - \ell_2^2 & = & 0 \end{array} \tag{69}$$

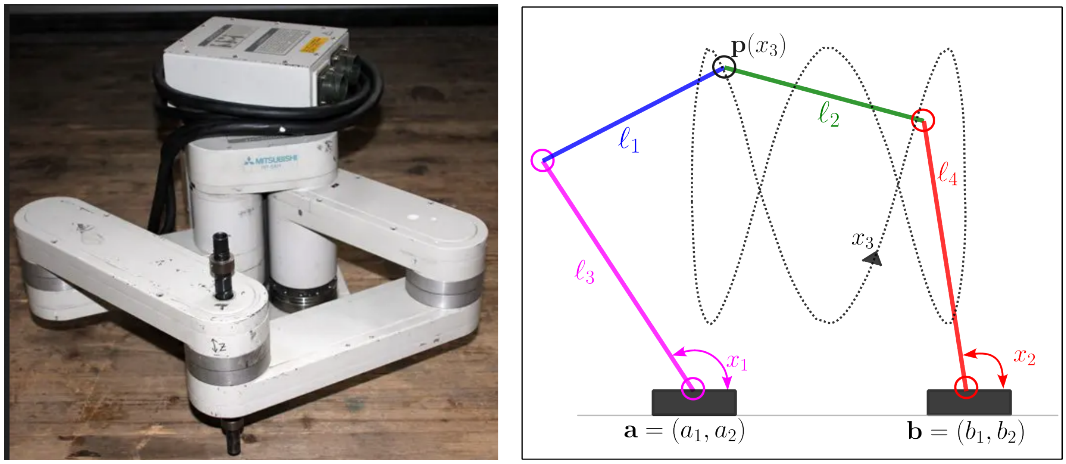

Figure 13: Left: RP-5AH Robot (Courtesy of Mitsubishi Electric Corporation). Right: The point $\mathbf{p}$ should stay on the Lissajou curve

Using our algorithm for $\varepsilon = 2^{-6}$, in less than 1 sec, we get Figure 14, right, to be compared with the continuation method (left) obtained by [14]. The frame box is taken as

$$[\mathbf{x}] = [-0.6, 2.5] \times [0.7, 2.1] \times [0, 2\pi]. \tag{70}$$

Note that the continuation method is also based on parallelepipeds, but may loose solutions. This is the case for this example as we can see if we compare carefully the top on the two figures. We can observe indeed that two tiny pieces of solution, shaped like a needle, exist on the right figure. These two needle tips do not appear on the left figure. The reason for this is that the basin of attraction near to these two needle tips is so small that it has been missed by the continuation method.

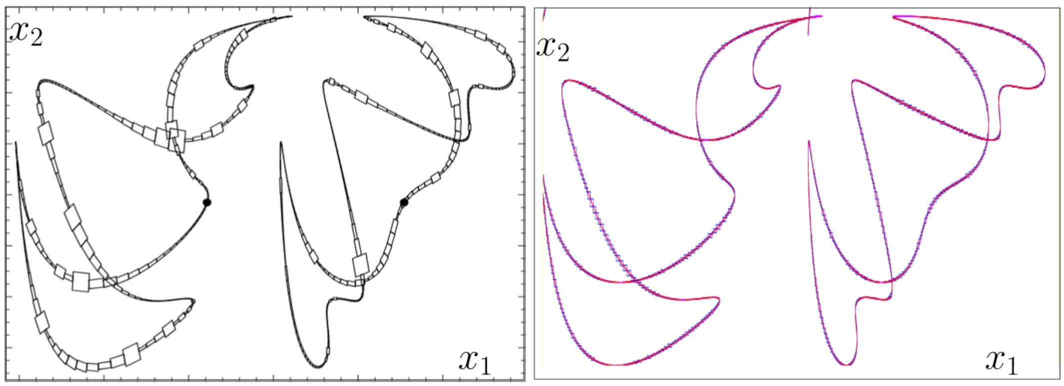

Figure 14: Solution set of the two armed problem in the (x_1, x_2) space; Left: continuation method, Right: with gutters

In the workspace, a discrete approximation of the occupancy set is depicted on Figure 15.

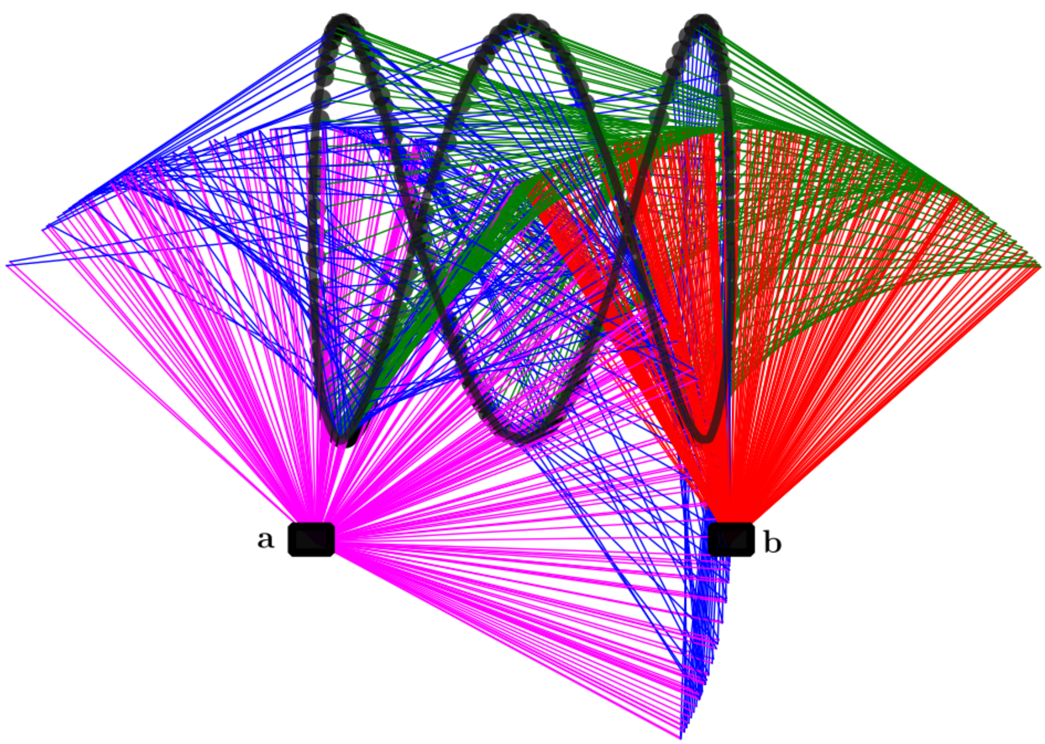

Figure 15: Occupancy set in the workspace

The code source of the test cases is based on the codac library [21] and can be found at:

https://webperso.ensta.fr/jaulin/gutter.html

6 Conclusion

In this paper, we have introduced a new abstract domain called a *gutter* to characterize the solution set of nonlinear equations. A gutter $\langle[\mathbf{x}], \mathbf{A}, \mathbf{b}, \rho\rangle$ is composed of a box $[\mathbf{x}]$, a flat $\mathbf{A}\mathbf{x}+\mathbf{b}=\mathbf{0}$ and a radius ρ.

- The box $[\mathbf{x}]$ is needed to obtain non-overlapping wrappers.
- The flat is needed to define the linear approximation and obtain a first-order approximation
- The radius ρ is needed to have the guarantee.

This new wrapper improves approximation accuracy, compared to classical interval techniques. Moreover, gutters are easy to project and intersect, which is not the case for other first-order approximations such as parallelotopes, ellipsoids, zonotopes.

Three test cases taken from the literature have shown the efficiency of gutters and the accuracy of the approximation that could be obtained.

References

[1] M. Arsenault. *Développement et analyse de mécanismes de tenségrité*. PhD thesis, Université Laval, Québec, Canada, 2006. Thèse de doctorat.

[2] M. Berger. *Espaces euclidiens, triangles, cercles et sphères*, volume 2 of *Géométrie*. Cedic/Fernand Nathan, Paris, France, 1979.

[3] A. Chapoutot and J. Alexandre dit Sandretto. Validated explicit and implicit Runge-Kutta methods. *Reliable Computing*, 22(1):79–103, July 2016.

[4] C. Combastel. A state bounding observer for uncertain non-linear continuous-time systems based on zonotopes. In *Proceedings of the 44th IEEE Conference on Decision and Control (CDC)*, pages 7228–7234. IEEE, 2005.

[5] P. Cousot and R. Cousot. Abstract interpretation: A unified lattice model for static analysis of programs by construction or approximation of fixpoints. In *Conference Record of the Fourth ACM Symposium on Principles of Programming Languages*, pages 238–252, Los Angeles, California, 1977.

[6] M. Godard, L. Jaulin, and D. Masse. Inner and outer approximation of the image of a set by a nonlinear function. *International Journal of Approximate Reasoning*, 187:109574, 2025.

[7] E. R. Hansen. *Global Optimization using Interval Analysis.* Marcel Dekker, New York, NY, 1992.

[8] M. Hladík. Enclosures for the solution set of parametric interval linear systems. *International Journal of Applied Mathematics and Computer Science*, 22(3):561–574, 2012.

[9] L. Jaulin. Asymptotically minimal interval contractors based on the centered form. *Acta Cybernetica*, 26(4):933–954, 2024.

[10] L. Jaulin, M. Kieffer, O. Didrit, and E. Walter. *Applied Interval Analysis, with Examples in Parameter and State Estimation, Robust Control and Robotics.* Springer-Verlag, London, 2001.

[11] L. Jaulin and E. Walter. Guaranteed nonlinear estimation and robust stability analysis via set inversion. In *Proceedings of the 2nd European Control Conference*, pages 818–821, 1993.

[12] V. Kreinovich, A.V. Lakeyev, J. Rohn, and P. Kahl. Computational complexity and feasibility of data processing and interval computations. *Reliable Computing*, 4(4):405–409, 1998.

[13] A. Kurzhanski and I. Valyi. *Ellipsoidal Calculus for Estimation and Control.* Birkhäuser, Boston, MA, 1997.

[14] B. Martin, A. Goldsztejn, L. Granvilliers, and C. Jermann. Certified parallelotope continuation for one-manifolds. *SIAM Journal on Numerical Analysis*, 51(6):3373–3401, 2013.

[15] A. Miné. The octagon abstract domain. *Higher Order Symbol. Comput.*, 19(1):31–100, 2006.

[16] R. Moore. *Methods and Applications of Interval Analysis.* Society for Industrial and Applied Mathematics, jan 1979.

[17] H. Ratschek and J. Rokne. *New Computer Methods for Global Optimization.* Ellis Horwood, Chichester, UK, 1988.

[18] A. Rauh and E. Auer. *Modeling, Design, and Simulation of Systems with Uncertainties.* Springer, 2011.

[19] B. Rego, D. Raimondo, and G. Raffo. Set-based state estimation of nonlinear systems using constrained zonotopes and interval arithmetic. In *2018 European Control Conference (ECC)*, pages 1584–1589. IEEE, June 2018.

[20] N. Revol. Introduction to the IEEE 1788-2015 Standard for Interval Arithmetic. *10th International Workshop on Numerical Software Verification - NSV 2017*, 2017.

[21] S. Rohou, B. Desrochers, and F. Le Bars. The codac library. *Acta Cybernetica*, 26(4):871–887, 2024.

[22] S. M. Rump. INTLAB - INTerval LABoratory. In Tibor Csendes, editor, *Developments in Reliable Computing*, pages 77–104. Kluwer, Dordrecht, the Netherlands, 1999.

[23] J. Scott, D. Raimondo, G. Marseglia, and R. Braatz. Constrained zonotopes: A new tool for set-based estimation and fault detection. *Automatica*, 69:126–136, 2016.

[24] V. Turkulov, M.R. Rapaić, and R. Malti. Stability analysis of time-delay systems in the parametric space. *Automatica*, 157, 2023.

[25] J. Wan. *Computationally reliable approaches of contractive model predictive control for discrete-time systems.* PhD dissertation, Universitat de Girona, Girona, Spain, 2007.

[26] P. Wenger and D. Chablat. Kinetostatic analysis and solution classification of a class of planar tensegrity mechanisms. *Robotica*, 37(7):1214–1224, 2019.